Electronic Supplementary Information (ESI)

Synergistic effect between atomically dispersed Fe and Co metal sites for enhanced oxygen reduction reaction

Lulu Chen,[a,b] Yelong Zhang,[c] Lile Dong,[a] Wenxiu Yang,[e] Xiangjian Liu,[a,b] Ling Long,[a,b] Changyu Liu,*[d] Shaojun Dong *[a,b] and Jianbo Jia *[a,b,d]

[a] State Key Laboratory of Electroanalytical Chemistry, Changchun Institute of Applied Chemistry, Chinese Academy of Sciences, Changchun 130022, China.

[b] University of Science and Technology of China, Hefei 230026, China.

[c] School of Applied Physics and Materials, Wuyi University, Jiangmen 529020, China.

[d] School of Biotechnology and Health Sciences, Wuyi University, Jiangmen 529020, China.

[e] School of Materials Science and Engineering, Beijing Institute of Technology, Beijing 100081 China.

* Corresponding author

Changyu Liu − Email: cyliu@ciac.ac.cn;

Shaojun Dong − Email: dongsj@ciac.ac.cn;

Jianbo Jia − Email: jbjia@ciac.ac.cn or jbjia@wyu.edu.cn

Experimental section

Characterization: Atomic-resolution spherical aberration corrected scanning transmission electron microscope (AC-TEM) image was achieved using FEI Titan Cubed Themis G2 300. Transmission electron microscope (TEM) images, high resolution TEM images, and elemental mapping images were obtained from FEI TECNAI G2. An XL 30 ESEM FEG SEM was employed to acquire scanning electron microscopy (SEM) images. X-ray diffraction (XRD) patterns of the samples were carried out on a Bruker D8 ADVANCE. X-ray photoelectron spectroscopy (XPS) was obtained from ESCALAB 250. Inductively coupled plasma optical emission spectrometry (ICP-OES) was performed on iCAP 6000 SERIES (Thermo Scientific, USA). Nitrogen adsorption-desorption isothermals were performed on ASAP 2020 Physisorption Analyzer. X-ray absorption near-edge structures (XANES) of the catalysts were conducted on 1W2B end station, Beijing Synchrotron Radiation Facility (BSRF). The K-edge spectra of Fe and Co were obtained at room temperature in transmission mode. The electrochemical measurements were carried out on CHI 842B work stations. Rotating ring-disk electrode (RRDE) techniques were performed on a Model RRDE-3A Apparatus.

Equations in Electrochemical characterization

The HO_2^- yield (HO_2^-%) and electron transfer number (n) of the catalysts were obtained from the equations:

$$HO_2^- \% = \frac{200\frac{I_r}{N}}{I_d + \frac{I_r}{N}}$$

$$n = \frac{4I_d}{I_d + \frac{I_r}{N}}$$

As the current collection efficiency, N was determined to be 0.44. I_d and I_r were the detected current on the disk and ring electrodes, respecctively. LSV curves at different rotating speed were recorded to calculate the electron transfer number by the Koutecky-Levich equation:

$$\frac{1}{J} = \frac{1}{J_L} + \frac{1}{J_K} = \frac{1}{B\omega^{1/2}} + \frac{1}{J_K}$$

$$B = 0.62nFC_0(D_0)^{2/3}V^{-1/6}$$

where J is the measured current density, J_K and J_L are the kinetic and limiting current densities, ω is the angular velocity of the rotating disk, n is the electron transfer number, F is the Faraday constant (96485 C mol^{-1}), C_o is the bulk concentration of O_2 in 0.10 M KOH solution (1.2×10^{-6} mol cm^{-3}), D_o is the diffusion coefficient of O_2 (1.9×10^{-5} cm^2 s^{-1}), and V is the kinematic viscosity of 0.10 M KOH solution (0.01 cm^2 s^{-1}).

The free energy changes of ORR: Free energy changes from initial states to final states of the reaction is calculated as follows:

$$\Delta G = \Delta E + \Delta ZPE - T\Delta S + \Delta G_U + \Delta G_{pH}$$

Where ΔE is the total energy change based on the DFT calculations, ΔZPE and ΔS are the changes in zero-point energy and in entropy, respectively. T is room temperature

(298.15 K). ΔG=-eU, where U is the electrode potential with respect to standard hydrogen electrode, and e is the transferred charge. $^{\Delta G_{pH}} = k_B T ln10 \times pH$, where k_B is the Boltzmann constant. Pervious study indicated that the theoretical working potential is independent of the pH, because the free energies for the elementary reactions vary in the same way with pH, thereby the potential determining step remains the same.[1] Therefore, to simplify the simulating results, the pH=0 is employed. The free energy of O_2 is obtained from the free energy change of the reaction $O_2+2H_2 \rightarrow 2H_2O$, which is -4.92 eV at 298.15 K and a pressure of 0.035 bar.[2] The free energy of $(H^+ + e^-)$ at standard conditions is assumed as the energy of $1/2H_2$.[2, 3] The entropy of the H_2 is taken from the NIST database, while the entropies of the ORR intermediates are calculated from the vibrational frequencies.[4]

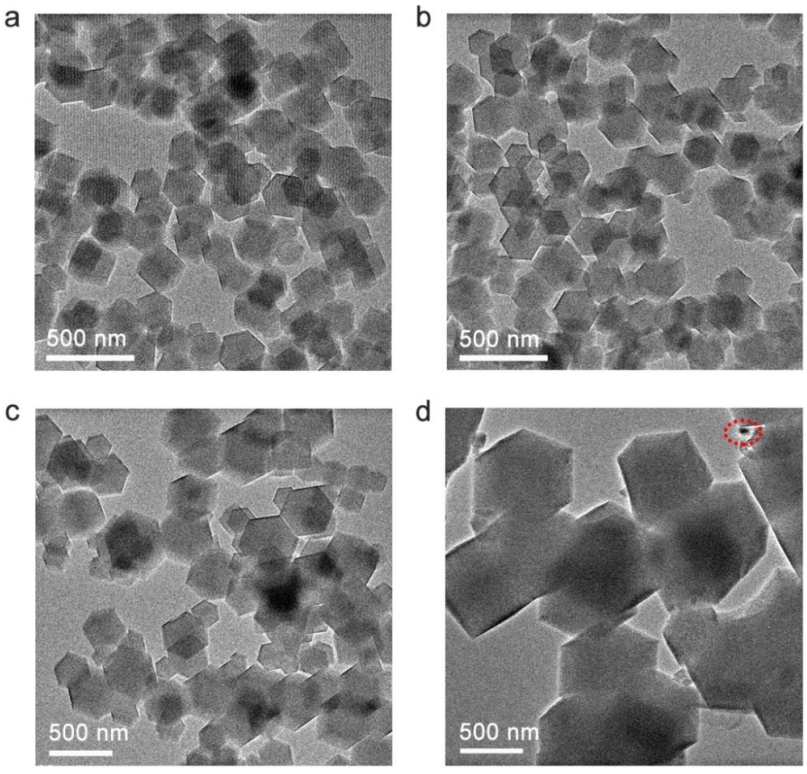

Figure S1. TEM images of (a) X_{100}-900, (b) X_{80}-900, (c) X_{40}-900, and (d) X_{20}-900. The red circle in d shows the Co nanoparticles in X_{20}-900.

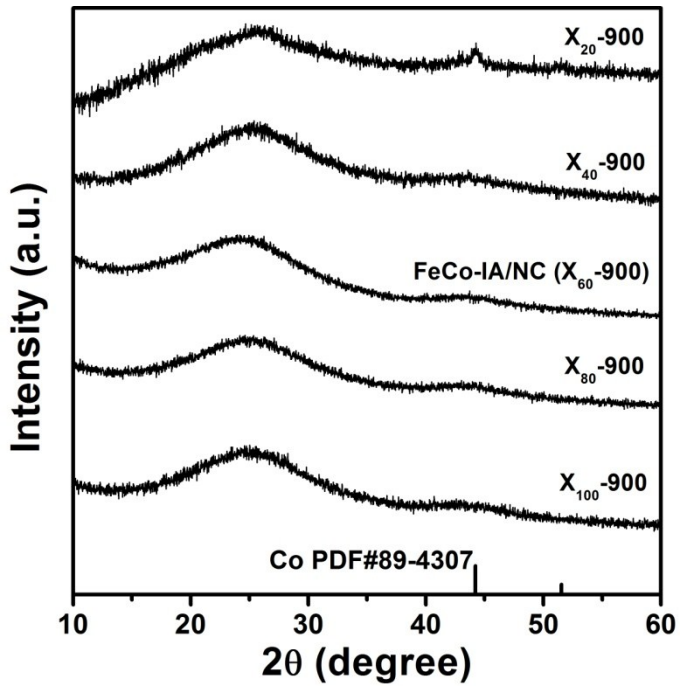

Figure S2. XRD patterns of X_{100}-900, X_{80}-900, Fe-IA/NC (X_{60}-900), X_{40}-900, and X_{20}-900.

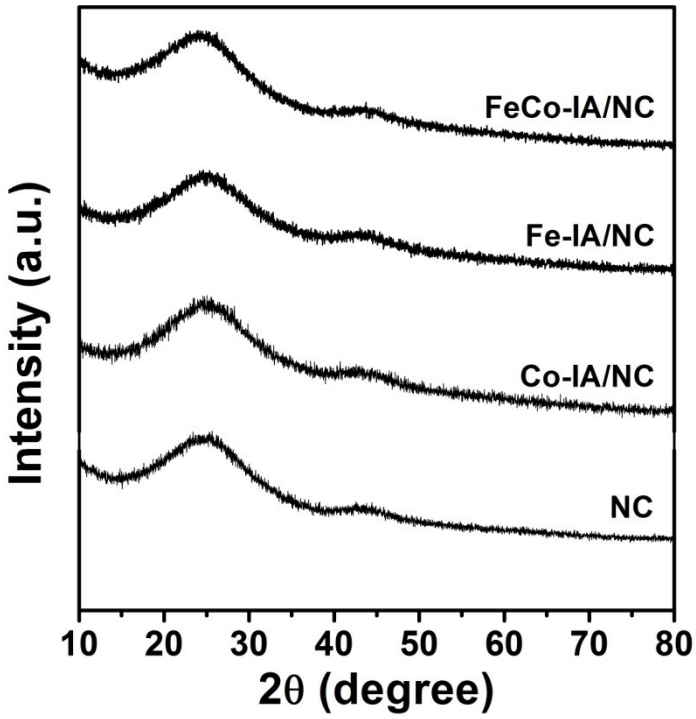

Figure S3. XRD patterns of FeCo-IA/NC, Fe-IA/NC, Co-IA/NC, and NC.

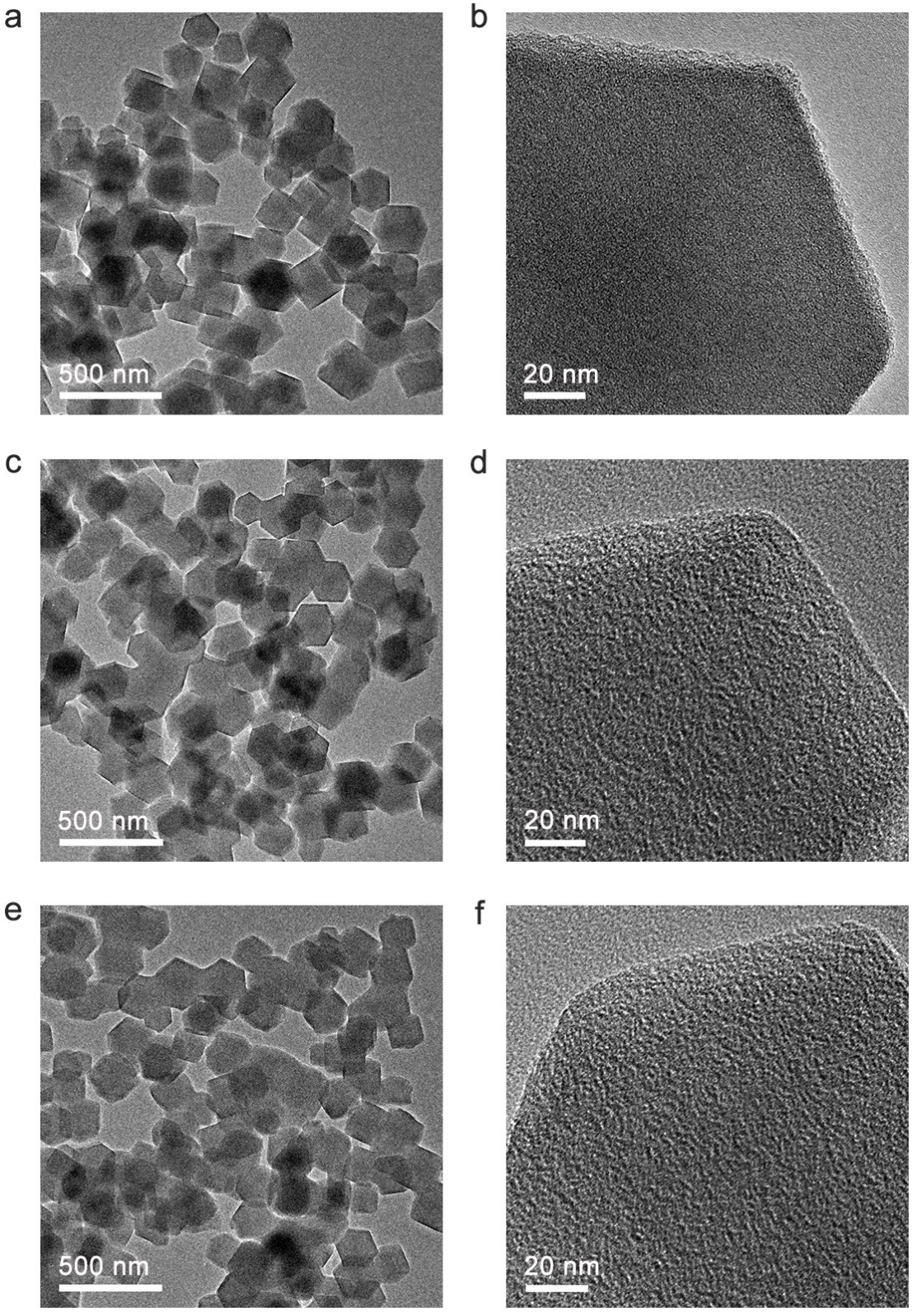

Figure S4. TEM images of (a-b) Fe-IA/NC, (c-d) Co-IA/NC, and (e-f) NC.

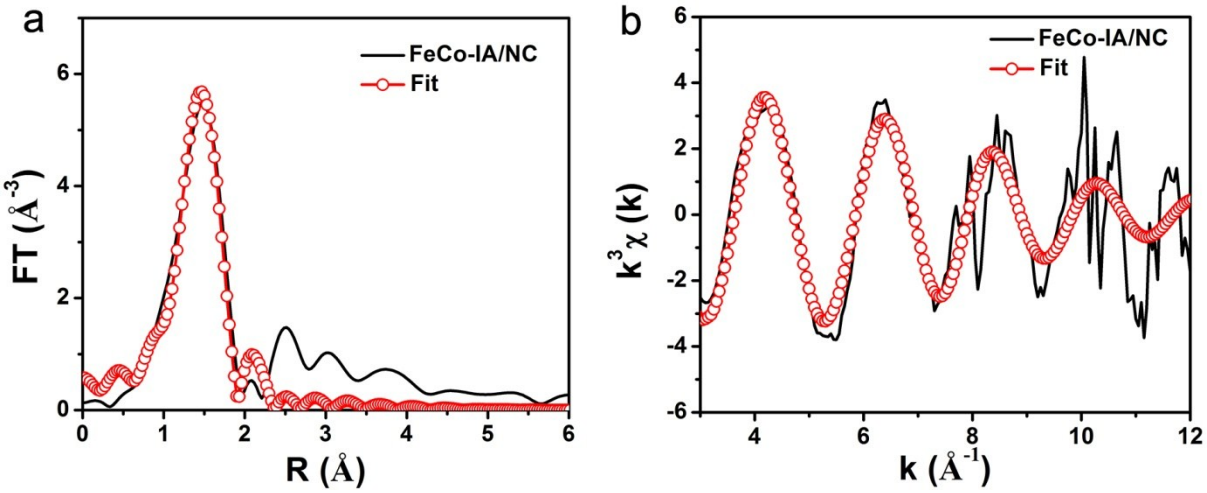

Figure S5. The corresponding EXAFS fitting curves of the FeCo-IA/NC in (a) R space and (b) k space at Fe K-edge.

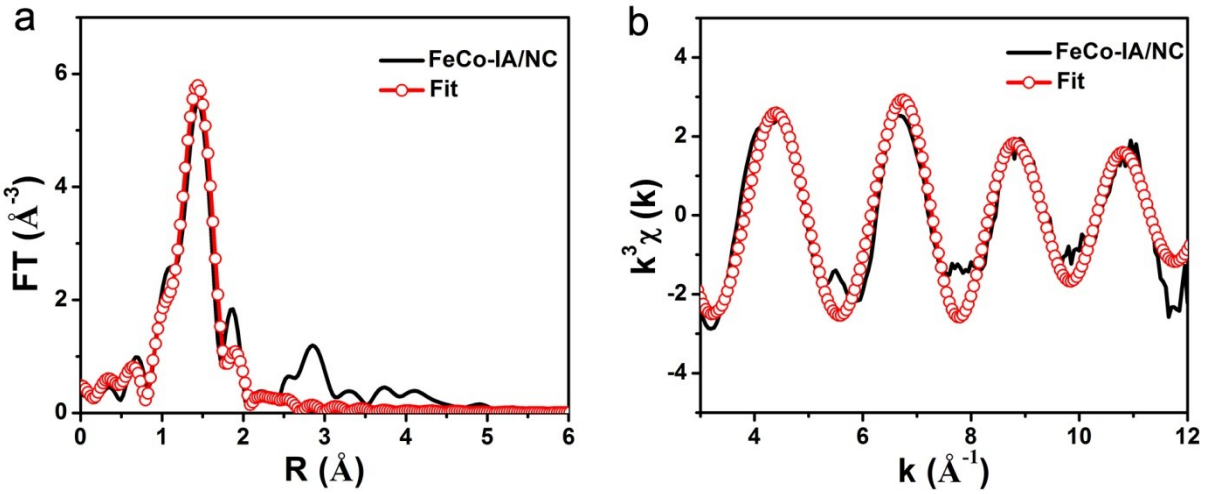

Figure S6. The corresponding EXAFS fitting curves of the FeCo-IA/NC in (a) R space and (b) k space at Co K-edge.

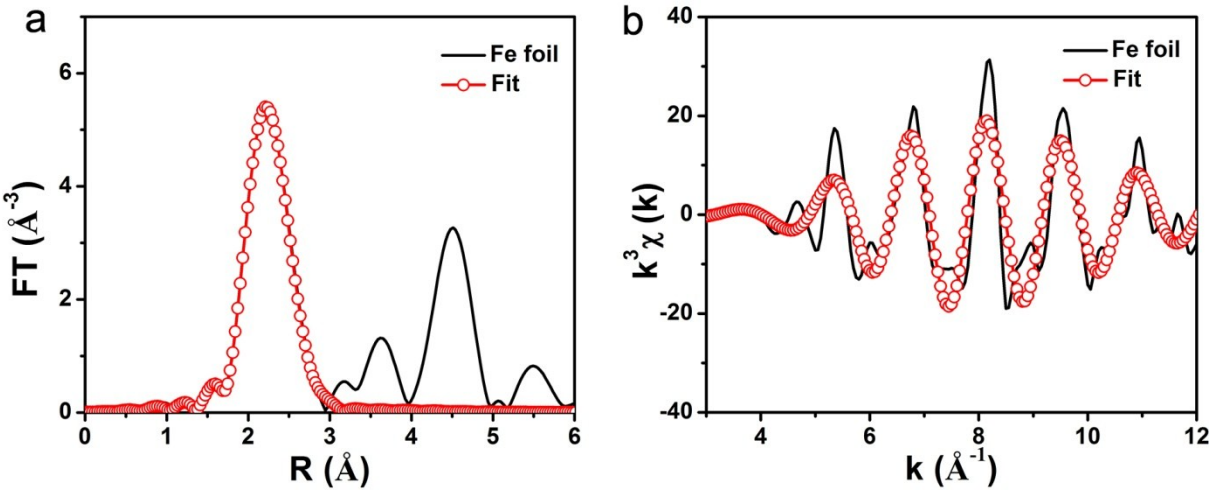

Figure S7. The corresponding EXAFS fitting curves of the Fe foil in (a) R space and (b) k space at Fe K-edge.

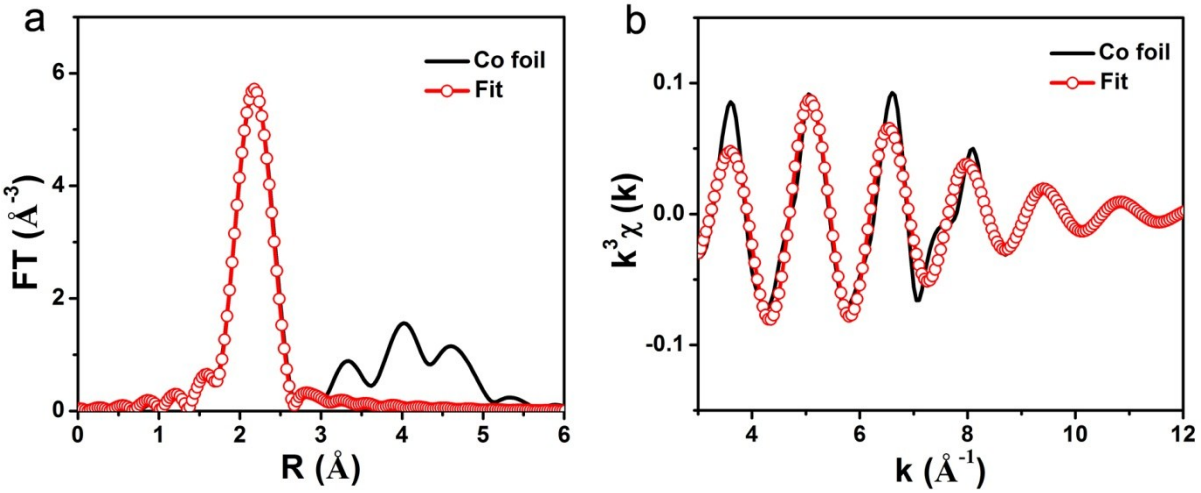

Figure S8. The corresponding EXAFS fitting curves of the Co foil in (a) R space and (b) k space at Co K-edge.

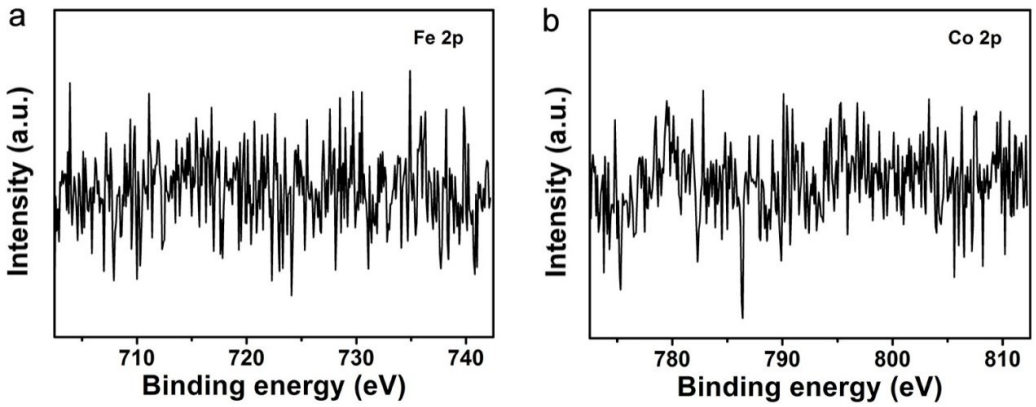

Figure S9. High resolution XPS spectra of (a) Fe and (b) Co in FeCo-IA/NC.

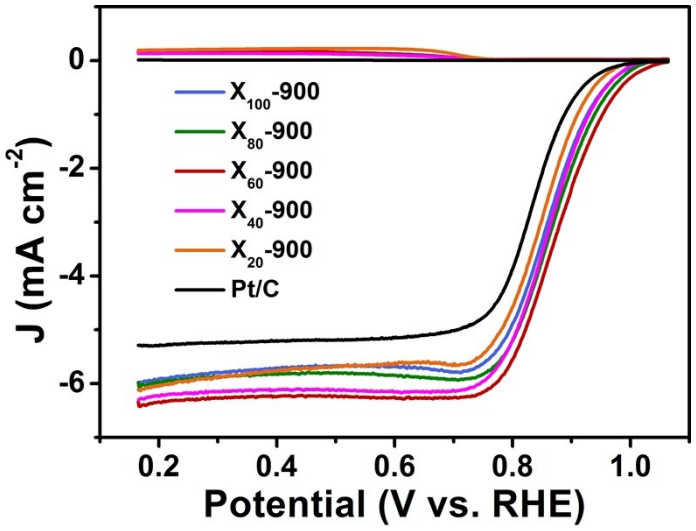

Figure S10. RRDE curves of samples with different metal content (X = 100, 80, 60, 40, and 20) and the commercial Pt/C in O_2-saturated 0.10 M KOH with the scan rate of 5 mV s^{-1} and rotating speed of 1600 rpm.

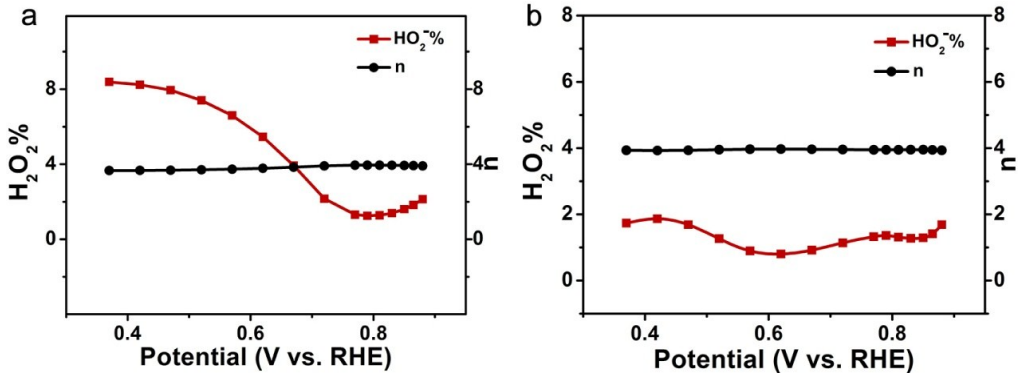

Figure S11. HO_2^-% and electron transfer number (n) of (a) FeCo-IA/NC and (b) Pt/C.

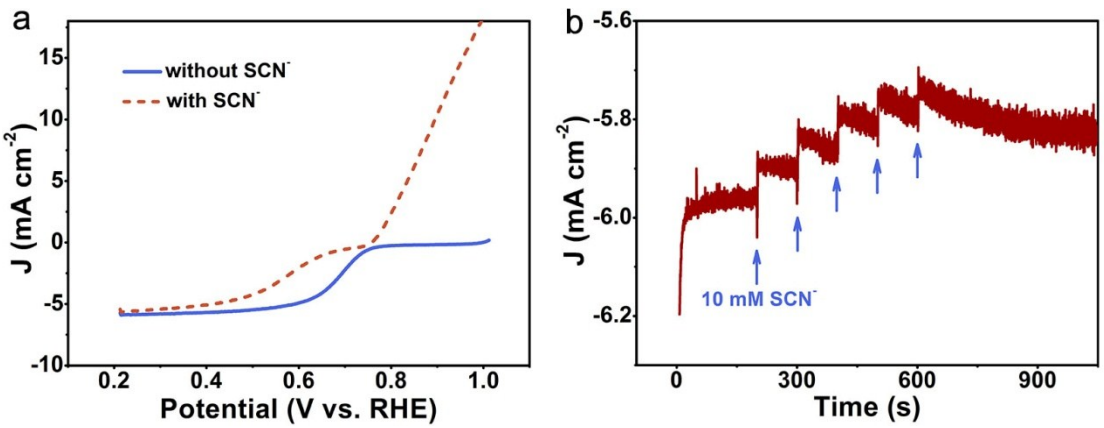

Figure S12. (a) LSV curves of FeCo-IA/NC for ORR before and after addition of 10 mM SCN^- into 0.50 M H_2SO_4. (b) I-t curve of FeCo-IA/NC for ORR with addition of SCN^- into 0.50 M H_2SO_4.

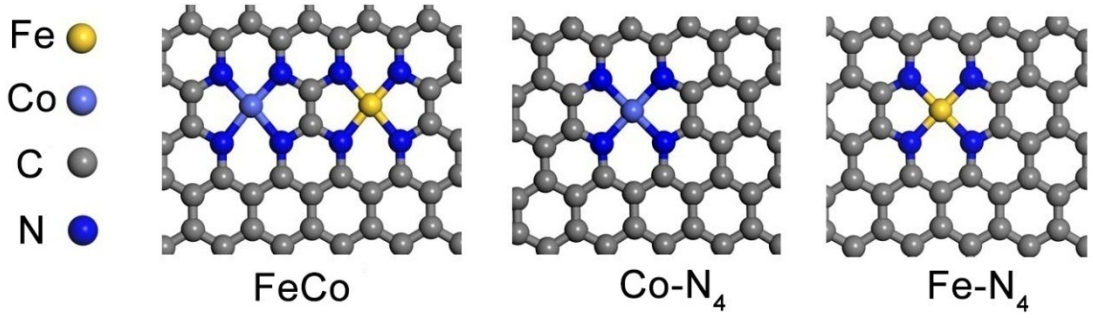

Figure S13. Structure models for FeCo-IA/NC (FeCo), Co-IA/NC (Co-N_4), and Fe-IA/NC (Fe-N_4).

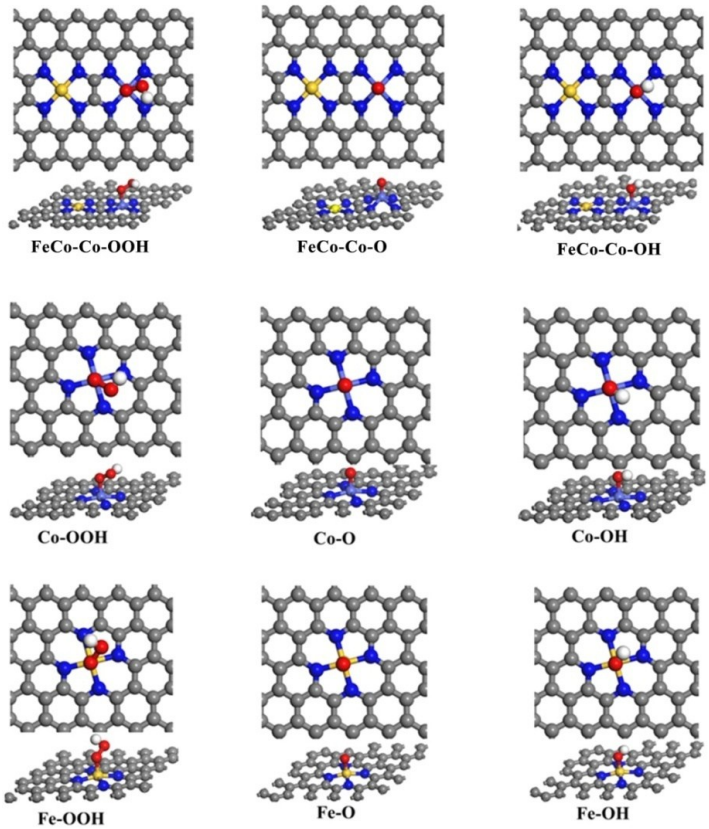

Figure S14. The adsorption structures for OOH, O, and OH in ORR process of the established configurations.

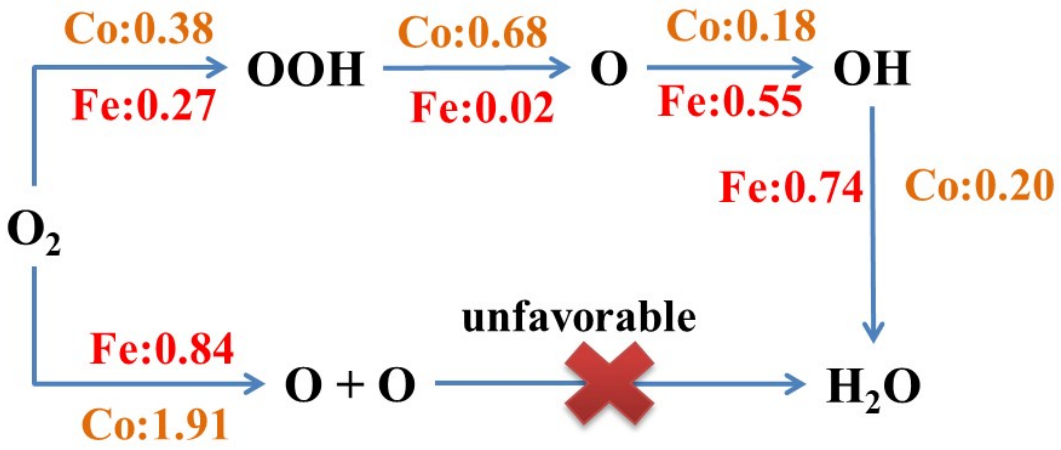

Figure S15. The barriers for the possible elementary reactions on FeCo structure. We calculated the elementary barriers for the mechanism of $O_2 \rightarrow OOH \rightarrow O \rightarrow OH \rightarrow H_2O$ (association pathway, denoted as path 1) and $O_2 \rightarrow 2O \rightarrow 2OH \rightarrow H_2O$ (dissociation pathway, denoted as path 2). The detailed computational methods are shown in Fig. S16-17. It is seen that the elementary reaction of $O_2 \rightarrow 2O$ shows

higher barrier than that of $O_2 + H \rightarrow OOH$. This suggests that the path 1 is favored in ORR, compared to path 2. Furthermore, other elementary reaction barriers in path 1 are lower than O_2 dissociation, which further proves that the path 1 will be the main channel for the ORR on FeCo structure. In addition, many reported literatures have demonstrated that FeN_4 and CoN_4 structures take association pathway for the ORR by calculating activation barriers.[5-8]

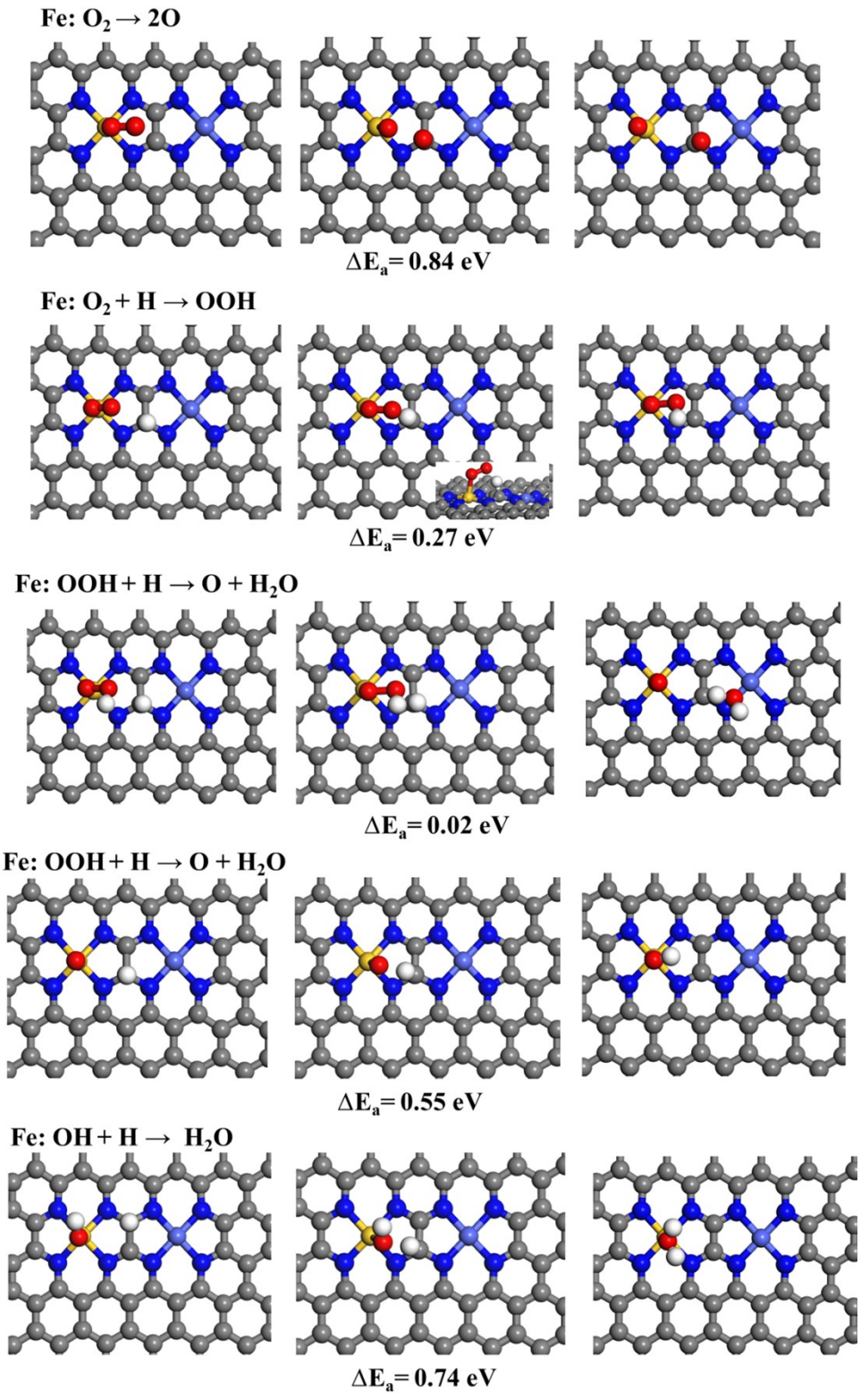

Figure S16. The structures for elementary reactions in ORR on Fe center of FeCo.

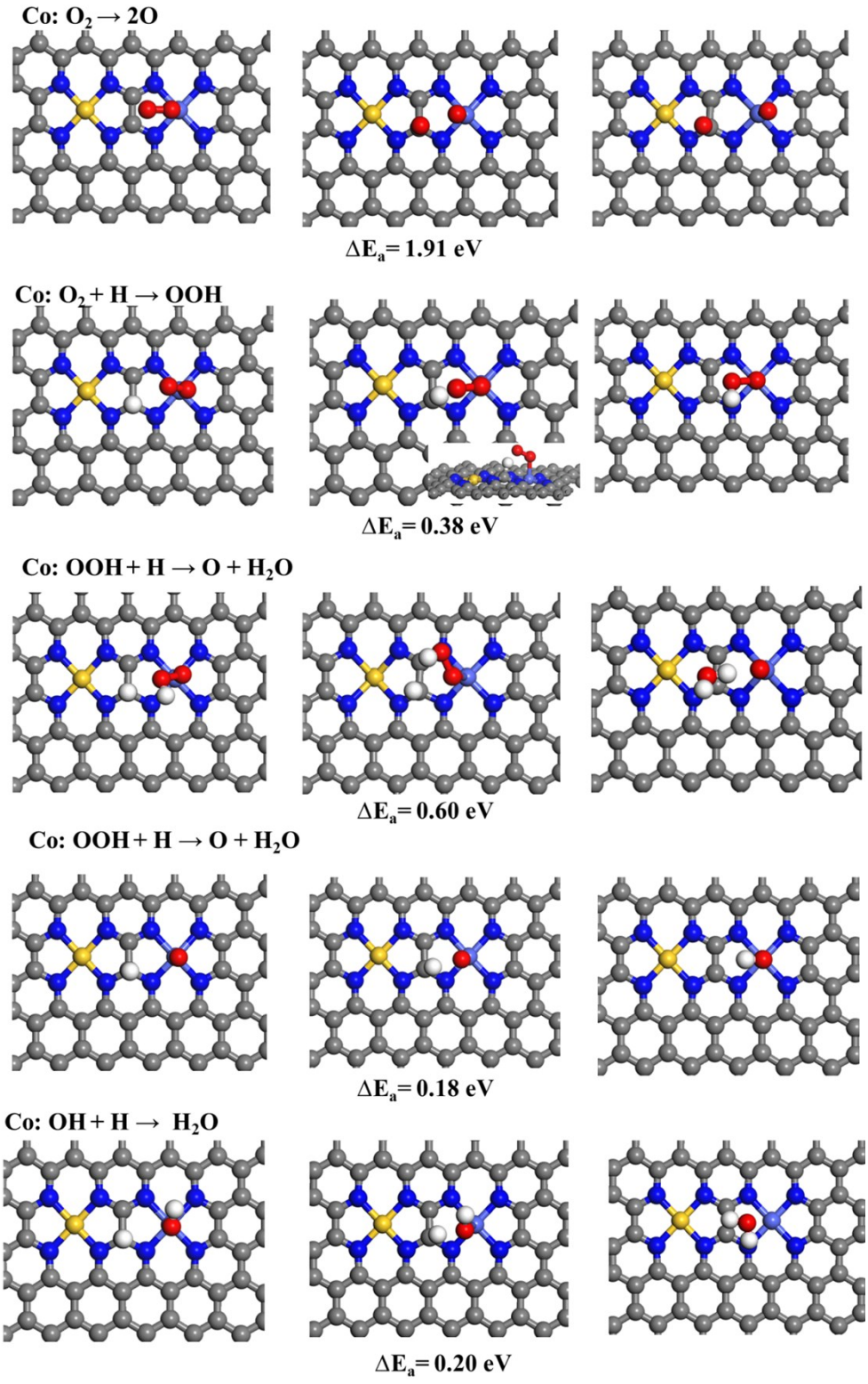

Figure S17. The structures for elementary reactions in ORR on Co center of FeCo.

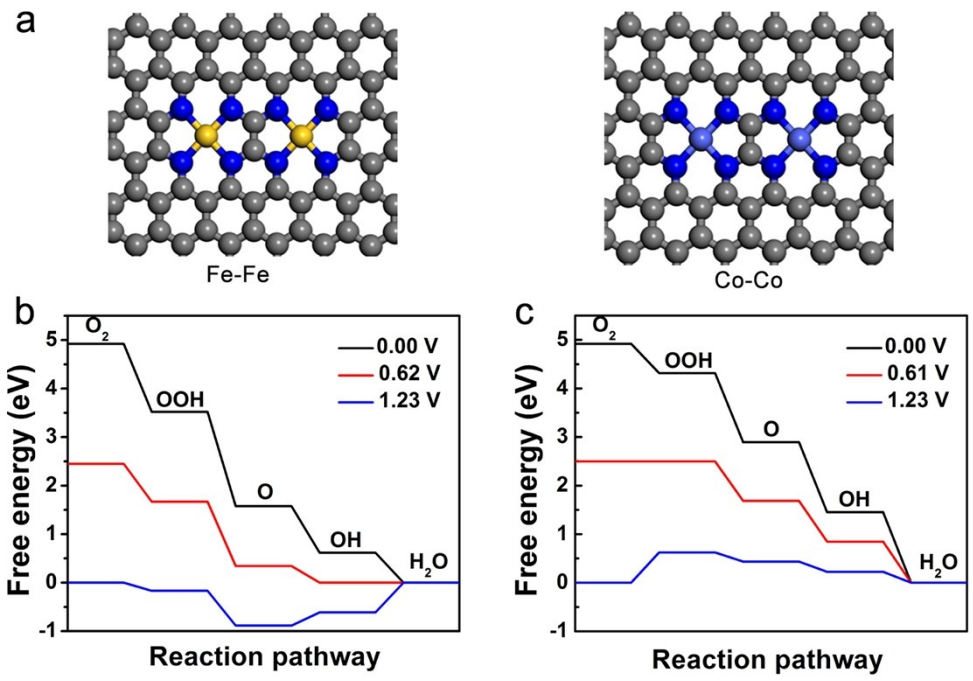

Figure S18. The structure models (a) and the free energy changes of ORR on (b) Fe-Fe and (c) Co-Co structures.

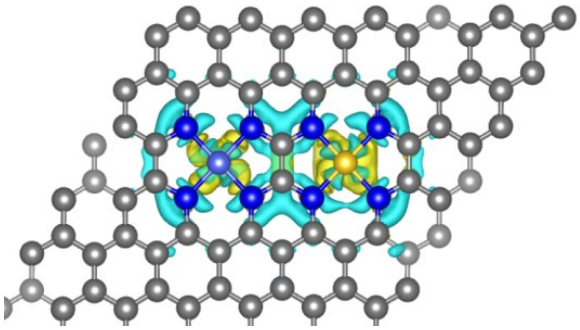

Figure S19. Differential charge density distribution on the structure model of FeCo. The yellow and blue areas denote the charge depletion and accumulation, respectively. The isosurface value of differential charge density distribution is 0.003 e/Å^3.

Figure S20. Photograph of the Zn-air battery employing the commercial cathode, giving an open-circuit potential of 1.385 V.

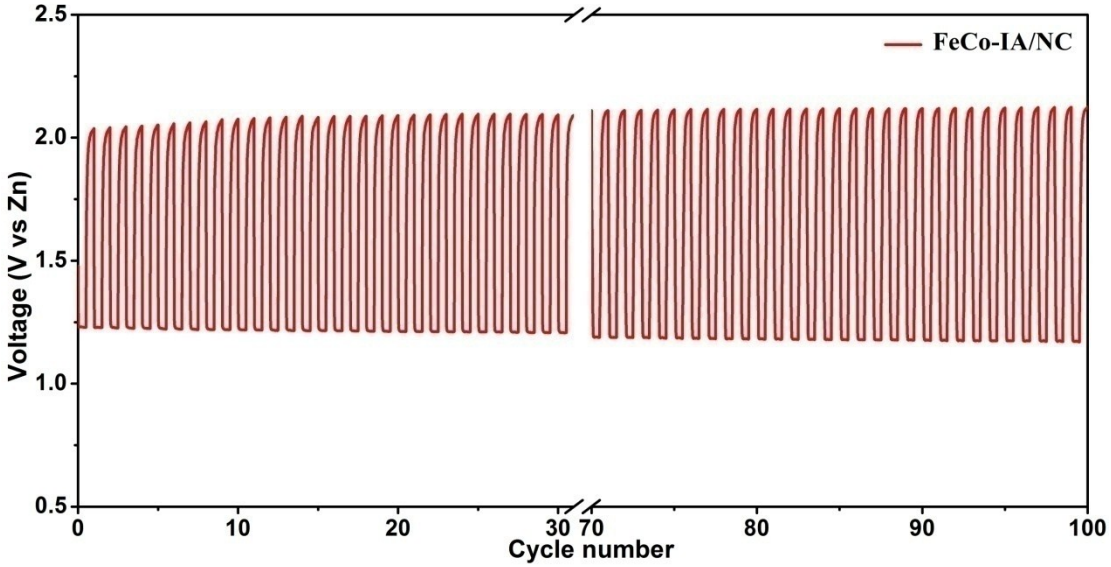

Figure S21. Charge/discharge curves of the Zn-air battery with FeCo-IA/NC as the air electrodes at a current density of 10 mA cm^{-2} (20 min per cycle).

Table S1. EXAFS fitting parameters at the Fe and Co K-edge EXAFS fitting of FeCo-IA/NC. (S_0^2=0.82)

Sample	Path	CN	R (Å)	σ^2 (Å^2)	ΔE_0 (eV)	R factor
Fe foil	Fe-Fe	8*	2.47±0.01	0.004	6.6±1.3	0.002
	Fe-Fe	6*	2.85±0.01	0.006	5.3±2.7	
Sample-Fe	Fe-N	4.1±0.9	1.99±0.01	0.009	-1.8±2.3	0.015
Co foil	Co-Co	12*	2.49±0.00	0.006	7.2±0.5	0.002
Sample-Co	Co-N	4.3±0.5	1.90±0.01	0.008	5.2±2.7	0.006

CN: coordination numbers; *R*: bond distance; σ^2: Debye-Waller factors; ΔE_0: the inner potential correction. *R* factor: goodness of fit. * the experimental EXAFS fit of metal foil by fixing CN as the known crystallographic value.

Table S2. The doping content of Fe and Co in the samples characterized by ICP-OES.

Sample	Fe (wt %)	Co (wt %)
X_{100}-900	0.08	0.45
X_{80}-900	0.15	0.76
FeCo-IA/NC (X_{60}-900)	0.26	1.06
X_{40}-900	0.33	1.28
X_{20}-900	0.42	1.51
Fe-IA/NC	0.23	-
Co-IA/NC	-	1.02

Table S3. The comparison of ORR activities (E_{onset} and $E_{1/2}$) of the samples with different metal content (X = 100, 80, 60, 40, and 20).

Sample	E_{onset} (V)	$E_{1/2}$ (V)
X_{100}-900	1.00	0.86
X_{80}-900	1.01	0.87
FeCo-IA/NC (X_{60}-900)	1.03	0.88
X_{40}-900	1.00	0.86
X_{20}-900	0.99	0.85

Table S4. Comparison of the ORR activity of FeCo-IA/NC with recently reported isolated metal atoms doped carbon catalysts in 0.10 M KOH. It can be observed that FeCo-IA/NC is one of the most active isolated transition metal atoms doped carbon catalysts for ORR.

Catalyst	E_{onset} (V)	$E_{1/2}$ (V)	Ref.
Single Co atoms on N-doped carbon	0.97	0.845	[9]
Single Fe atoms on N-doped carbon	1.046	0.87	[10]
Isolated Zn-Co atomic pair on N-doped carbon	1.004	0.861	[11]
Single Co atoms on N-doped carbon flake arrays/carbon nanofibers	-	0.88	[12]
Single Fe atoms on N-doped carbon nanotube aerogels	0.97	0.88	[13]
Single Fe atoms on N-doped carbon	0.954	0.834	[14]
Single Fe atoms on N,S codoped carbon	-	0.85	[15]
Single Co atoms on N-doped carbon	0.982	0.881	[16]
Single Fe atoms on 2D N-doped carbon	-	0.853	[17]
Single Fe atoms on N-doped carbon	-	0.869	[18]
Single Fe atoms on N-doped carbon	0.972	0.885	[19]
Single Co atoms on g-C_3N_4	0.90	0.85	[20]
Isolated Fe and Co atoms dual sites on N-doped carbon	0.98	0.88	This work

Table S5. The energies employed in free energy diagram for ORR on the Fe site in FeCo.

U = 0.00 V						
	E_{DFT}	ZPE	TS	G	ΔG_U	ΔG
*	-627.94	0	0	-627.94	0.00	4.92
OOH*	-642.38	0.41	0.17	-642.13	0.00	4.17
O*	-633.19	0.06	0.08	-633.21	0.00	2.19
OH*	-637.87	0.37	0.10	-637.60	0.00	1.22
U=0.75 V						
*	-627.94	0	0	-627.94	0.00	1.90
OOH*	-642.38	0.41	0.17	-642.13	0.75	1.90
O*	-633.19	0.06	0.08	-633.21	0.75	0.68
OH*	-637.87	0.37	0.10	-637.60	0.75	0.47
U=1.23 V						
*	-627.94	0	0	-627.94	0.00	0.00
OOH*	-642.38	0.41	0.17	-642.13	1.23	0.48
O*	-633.19	0.06	0.08	-633.21	1.23	-0.27
OH*	-637.87	0.37	0.10	-637.60	1.23	-0.01

Table S6. The energies employed in free energy diagram for ORR on the Co site in FeCo.

U = 0.00 V						
	E_{DFT}	ZPE	TS	G	ΔG_U	ΔG
*	-627.94	0.00	0.00	-627.94	0.00	4.92
OOH*	-642.16	0.43	0.19	-641.91	0.00	4.39
O*	-633.12	0.06	0.07	-633.13	0.00	2.26

OH*	-637.69	0.35	0.10	-637.43	0.00	1.41
U=0.53 V						
*	-627.94	0.00	0.00	-627.94	0.00	2.79
OOH*	-642.16	0.43	0.19	-641.91	0.53	2.79
O*	-633.12	0.06	0.07	-633.13	0.53	1.19
OH*	-637.69	0.35	0.10	-637.43	0.53	0.88
U=1.23 V						
*	-627.94	0.00	0.00	-627.94	0.00	0.00
OOH*	-642.16	0.43	0.19	-641.91	1.23	0.70
O*	-633.12	0.06	0.07	-633.13	1.23	-0.20
OH*	-637.69	0.35	0.10	-637.43	1.23	0.18

Table S7. The energies employed in free energy diagram for ORR on the CoN_4.

U = 0.00 V						
	E_{DFT}	ZPE	TS	G	ΔG_U	ΔG
*	-442.75	0.00	0.00	-442.75	0.00	4.92
OOH*	-456.85	0.43	0.23	-456.65	0.00	4.45
O*	-446.85	0.06	0.07	-446.86	0.00	3.34
OH*	-452.41	0.34	0.12	-452.19	0.00	1.46
U=0.47 V						
*	-445.42	0.00	0.00	-445.42	0.00	3.05
OOH*	-459.86	0.43	0.21	-459.64	0.47	3.05
O*	-450.54	0.06	0.08	-450.56	0.47	2.41
OH*	-455.41	0.36	0.11	-455.16	0.47	0.99
U=1.23 V						
*	-445.42	0.00	0.00	-445.42	1.23	0.00

OOH*	-459.86	0.43	0.21	-459.64	1.23	0.76
O*	-450.54	0.06	0.08	-450.56	1.23	0.88
OH*	-455.41	0.36	0.11	-455.16	1.23	0.23

Table S8. The energies employed in free energy diagram for ORR on the FeN_4.

U = 0.00 V						
	E_{DFT}	ZPE	TS	G	ΔG_U	ΔG
*	-443.26	0.00	0.00	-443.26	0.00	4.92
OOH*	-458.19	0.43	0.19	-457.95	0.00	3.66
O*	-449.07	0.06	0.07	-449.08	0.00	1.64
OH*	-453.73	0.34	0.11	-453.50	0.00	0.65
U=0.65 V						
*	-443.26	0.00	0.00	-443.26	0.00	2.32
OOH*	-458.19	0.43	0.19	-457.95	0.65	1.71
O*	-449.07	0.06	0.07	-449.08	0.65	0.34
OH*	-453.73	0.34	0.11	-453.50	0.65	0.00
U=1.23 V						
*	-443.26	0.00	0.00	-443.26	1.23	0
OOH*	-458.19	0.43	0.19	-457.95	1.23	-0.03
O*	-449.07	0.06	0.07	-449.08	1.23	-0.82
OH*	-453.73	0.34	0.11	-453.50	1.23	-0.56

Table S9. The Bader charge (in e) for metal atoms in FeCo, FeN_4, and CoN_4 structures, respectively.

Structure	Fe	Co
FeN_4	6.9164	–
CoN_4	–	8.0893
FeCo	6.9537	7.8843

References

[1] I. C. Man, H. Y. Su, F. Calle‐Vallejo, H. A. Hansen, J. I. Martínez, N. G. Inoglu, J. Kitchin, T. F. Jaramillo, J. K. Nørskov, J. Rossmeisl, *ChemCatChem* **2011**, *3*, 1159-1165.

[2] J. K. Nørskov, J. Rossmeisl, A. Logadottir, L. Lindqvist, J. R. Kitchin, T. Bligaard, H. Jónsson, *J. Phys. Chem. B* **2004**, *108*, 17886-17892.

[3] M. Jiao, W. Song, K. Li, Y. Wang, Z. Wu, *J. Phys. Chem. C* **2016**, *120*, 8804-8812.

[4] J. D. Cox, D. D. Wagman, V. A. Medvedev, Hemisphere Publishing Corp., New York, 1984, 1.

[5] J. Zhang, Z. Wang, Z. Zhu, *J. Power Sources* **2014**, *255,* 65-69.

[6] S. Kattel, G. Wang, *J. Phys. Chem. Lett.* **2014**, *5*, 452-456.

[7] M. Xiao, H. Zhang, Y. Chen, J. Zhu, L. Gao, Z. Jin, J. Ge, Z. Jiang, S. Chen, C. Liu, W. Xing, *Nano Energy* **2018**, *46*, 396-403.

[8] F. Li, H. Shu, C. Hu, Z. Shi, X. Liu, P. Liang, X. Chen, *ACS Appl. Mater. Interfaces* **2015**, *7*, 27405-27413.

[9] Y. Deng, B. Chi, X. Tian, Z. Cui, E. Liu, Q. Jia, W. Fan, G. Wang, D. Dang, M. Li, K. Zang, J. Luo, Y. Hu, S. Liao, X. Sun, S. Mukerjee, *J. Mater. Chem. A* **2019**, *7*, 5020-5030.

[10] Y. Chen, Z. Li, Y. Zhu, D. Sun, X. Liu, L. Xu, Y. Tang, *Adv. Mater.* **2019**, *31*, 1806312.

[11] Z. Lu, B. Wang, Y. Hu, W. Liu, Y. Zhao, R. Yang, Z. Li, J. Luo, B. Chi, Z. Jiang, M. Li, S. Mu, S. Liao, J. Zhang, X. Sun, *Angew. Chem. Int. Ed.* **2019**, *58*, 2622-2626.

[12] D. Ji, L. Fan, L. Li, S. Peng, D. Yu, J. Song, S. Ramakrishna, S. Guo, *Adv. Mater.* **2019**, 1808267.

[13] C. Zhu, S. Fu, J. Song, Q. Shi, D. Su, M. H. Engelhard, X. Li, D. Xiao, D. Li, L. Estevez, D. Du, Y. Lin, *Small* **2017**, *13*, 1603407.

[14] Q.-L. Zhu, W. Xia, L.-R. Zheng, R. Zou, Z. Liu, Q. Xu, *ACS Energy Lett.* **2017**, *2*, 504-511.

[15] P. Chen, T. Zhou, L. Xing, K. Xu, Y. Tong, H. Xie, L. Zhang, W. Yan, W. Chu, C. Wu, Y. Xie, *Angew. Chem. Int. Ed.* **2017**, *56*, 610-614.

[16] P. Yin, T. Yao, Y. Wu, L. Zheng, Y. Lin, W. Liu, H. Ju, J. Zhu, X. Hong, Z. Deng, G. Zhou, S. Wei, Y. Li, *Angew. Chem. Int. Ed.* **2016**, *55*, 10800-10805.

[17] C. Wang, W. Chen, K. Xia, N. Xie, H. Wang, Y. Zhang, *Small* **2019**, *15*, 1804966.

[18] J. Xie, B. Q. Li, H. J. Peng, Y. W. Song, J. X. Li, Z. W. Zhang, Q. Zhang, *Angew. Chem. Int. Ed.* **2019**, *58*, 4963-4967.

[19] Y. Pan, S. Liu, K. Sun, X. Chen, B. Wang, K. Wu, X. Cao, W. C. Cheong, R. Shen, A. Han, Z. Chen, L. Zheng, J. Luo, Y. Lin, Y. Liu, D. Wang, Q. Peng, Q. Zhang, C. Chen, Y. Li, *Angew. Chem. Int. Ed.* **2018**, *57*, 8614-8618.

[20] Y. Zheng, Y. Jiao, Y. Zhu, Q. Cai, A. Vasileff, L. H. Li, Y. Han, Y. Chen, S.-Z. Qiao, *J. Am. Chem. Soc.* **2017**, *139*, 3336-3339.